Supporting Information

Pentacosaple-CO_3^{2-} bridged hexacontaoctanuclear lanthanide-alkali barrels derived from octacosanuclear discs†

Chaolun Wei,[a] Yi Liu,[a] Xiaojuan Li,[a] Haoyu Liu,[a] Hai-Ye Li,*[c] Hou-Ting Liu*[b] and Haiquan Tian*[a]

[a] Shandong Provincial Key Laboratory of Chemical Energy Storage and Novel Cell Technology, School of Chemistry and Chemical Engineering, Liaocheng University, Liaocheng 252059, P. R. China.

[b] Food and Biochemistry Engineering Department, Yantai Vocational College, Yantai 264006, P. R. China.

[c] Key Laboratory for the Chemistry and Molecular Engineering of Medicinal Resources (Ministry of Education of China), School of Chemistry and Pharmacy, Guangxi Normal University, Guilin, 541004, P. R. China.

Table of Contents

S1 Materials and general procedures S5

S2 X-ray crystallography S5

S3 Structure information S6

Figure S1. Infrared spectra of $\mathbf{H_4L^1}$ (a) and $\mathbf{H_4L^2}$ (b). S6

Figure S2. Infrared spectra of compounds $\mathbf{Dy_{16}K_{12}}$ (a) and $\mathbf{Dy_{24}Na_{44}}$. S6

Figure S3. Thermal analysis of compounds $\mathbf{Dy_{16}K_{12}}$ (a) and $\mathbf{Dy_{24}Na_{44}}$ (b). S6

Figure S4. The powder XRD patterns of compound $\mathbf{Dy_{16}K_{12}}$ (a). The black circles are for the observed data (b). The red solid line is for the calculated data. The grey solid curve is for the difference. The vertical bars are the positions of Bragg peaks. Cell parameters: *R*-3*c*, a = 48.9298(8) Å, b = 48.9298(8) Å, c = 109.1024(3) Å, α = 90°, β = 90°, γ = 120°, V = 204065.86(1) Å^3 (wRp = 0.046). S7

Figure S5. The powder XRD patterns of compound $\mathbf{Dy_{24}Na_{44}}$ (a). The black circles are for the observed data (b). The red solid line is for the calculated data. The grey solid curve is for the difference. The vertical bars are the positions of Bragg peaks. Cell parameters: *P*2/*n*, a = 33.8050(1) Å, b = 33.8050(1) Å, c = 26.9287(6) Å, α = 90°, β =90°, γ = 90°, V = 30961.55(9) Å^3 (wRp = 0.058). S7

Figure S6. Ball-and-stick views of compound $\mathbf{Dy_{16}K_{12}}$ (a). Highlighting the $[Dy_{16}(L^1)_4(O_3P)_{16}(\mu_3\text{-}O)_4(\mu\text{-}O)_4]^{12-}$ fragment (b). The menaphthyl and ethyl groups, and the coordinating DMF, MeCN and H_2O molecules, and hydrogen atoms are omitted for clarity. ... S8

Figure S8. The coordination modes of the L^1 (a) and 1-naphthylphosphonate (b) ligands. S9

Figure S9. Space-filling representation of compound $\mathbf{Dy_{16}K_{12}}$ (a and b). S9

Figure S10. Ball-and-stick views of compound $\mathbf{Dy_{24}Na_{44}}$ (a). Highlighting the $[Dy_{24}(L^2)_8(O_3P)_{16}(CO_3)_{19}]^{30+}$ fragment (b). The menaphthyl and ethyl groups, and the coordinating DMF, MeCN and H_2O molecules, and hydrogen atoms are omitted for clarity.. S10

Figure S11. The coordination modes of the L^2 (a) and 1-naphthylmethylphosphonate (b) ligands. S10

Figure S12. Highlighting the $[Na_{44}(L^2)_8(O_3P)_{16}(CO_3)_{25}(Cl)_2(\mu_2\text{-}OH)_8]^{72-}$ fragment (a). The menaphthyl and ethyl groups, and the coordinating DMF, MeOH and H_2O molecules, and hydrogen atoms are omitted for clarity. Coordination polyhedra observed for the metal centers of compound $\mathbf{Dy_{24}Na_{44}}$ (b). S11

Figure S13. The coordination modes of the carbonate anions. S11

Figure S14. Space-filling representation of compound $\mathbf{Dy_{24}Na_{44}}$ (a and b). S12

Figure S15. Dissect the inorganic core motif of compound $\mathbf{Dy_{24}Na_{44}}$ into three concentric barrel-shaped shells. S12

Table S1. Selected bond lengths (Å) and angles (°) for compound $\mathbf{Dy_{16}K_{12}}$. S13

Table S2. Selected bond lengths (Å) and angles (°) for compound $\mathbf{Dy_{24}Na_{44}}$. S14

Table S3. Hydrogen bonds for compound $\mathbf{Dy_{16}K_{12}}$ S15

Table S4. Hydrogen bonds for compound $\mathbf{Dy_{24}Na_{44}}$. S15

Symmetry codes: a: x, y, 1/2-z; b: 2/3-x, 1/3+y, 2/3-z; c: -1/3+x, 1/3 -y, 2/3-z. S15

Table S5. Dy^{III} geometry analysis of $\mathbf{Dy_{16}K_{12}}$ by SHAPE 2.1 software. S16

Table S6. Dy^{III} geometry analysis of $\mathbf{Dy_{24}Na_{44}}$ by SHAPE 2.1 software. S16

S4 Magnetic properties S17

Figure S16. Temperature dependent of the $\chi_M T$ values at 1.0 kOe for compounds $\mathbf{Dy_{16}K_{12}}$ (a)

and **$Dy_{24}Na_{44}$** (b). Inset: the magnetization *vs.* field plots at different temperature. S17
Figure S17. Variable-field magnetization data collected for compounds **$Dy_{16}K_{12}$** (a) and **$Dy_{24}Na_{44}$** (b) at an average field sweep rate of 100 Oe/s. Inset shows a view of the plot at 1.8 K. S17
Figure S18. Variable-field χ_M' magnetic susceptibility versus frequency data for compounds **$Dy_{16}K_{12}$** (a) and **$Dy_{24}Na_{44}$** (b), collected at fields ranging from 0 to 0.4 T at 2.0 K.....S18
Figure S19. Variable-temperature χ_M' magnetic susceptibility versus frequency data for compound **$Dy_{16}K_{12}$** under zero applied dc field, collected at temperatures ranging from 1.8 to 18 K (a). Variable-frequency $\chi_M'T$ (b) and χ_M' (c) magnetic susceptibility versus temperature data under zero applied dc field, collected at frequencies from 1 to 999 Hz.....S18
Figure S20. Variable-temperature χ_M' magnetic susceptibility versus frequency data for compound **$Dy_{16}K_{12}$** under the optimal 0.2 T dc field, collected at temperatures ranging from 1.8 to 18 K (a). Variable-frequency $\chi_M'T$ (b) and χ_M' (c) magnetic susceptibility versus temperature data under the optimal 0.2 T dc field, collected at frequencies from 1 to 999 Hz.S19
Figure S21. Variable-temperature χ_M' magnetic susceptibility versus frequency data for compound **$Dy_{24}Na_{44}$** under zero applied dc field, collected at temperatures ranging from 1.8 to 18 K (a). Variable-frequency $\chi_M'T$ (b) and χ_M' (c) magnetic susceptibility versus temperature data under zero applied dc field, collected at frequencies from 1 to 999 Hz. 19
Table S7. Parameters used to fit temperature-dependent relaxation times for **$Dy_{16}K_{12}$** under zero applied dc field.....S20
Table S8. Parameters used to fit temperature-dependent relaxation times for **$Dy_{16}K_{12}$** under the optimal 0.2 T dc field.....S20
Table S9. Parameters used to fit temperature-dependent relaxation times for **$Dy_{24}Na_{44}$** under zero applied dc field.....S20
Table S10. Magnetization relaxation fitting parameters from least-squares fitting of $\chi(\omega)$ data for compound **$Dy_{16}K_{12}$** under the different applied dc field.....S21
Table S11. Magnetization relaxation fitting parameters from least-squares fitting of $\chi(\omega)$ data for compound **$Dy_{24}Na_{44}$** under the different applied dc field.....S21
Table S12. Relaxation fitting parameters from least-squares fitting of $\chi(\omega)$ data for compound **$Dy_{16}K_{12}$** under zero applied dc field.....S22
Table S13. The parameters obtained by fitting the Cole-Cole data of compound **$Dy_{16}K_{12}$** under the optimal 0.2 T dc field.....S23
Table S14. Relaxation fitting parameters from least-squares fitting of $\chi(\omega)$ data for compound **$Dy_{24}Na_{44}$** under zero applied dc field.....S24
S5 REFERENCES.....S25

S1 Materials and general procedures

All chemical reagents were purchased from commercial vendors and used without additional purification. The elemental analysis for C, H, and N were carried out in a $PE_{240}C$ elemental analyzer. The infrared spectra were recored as KBr pellets on a Bruker Tensor 27 spectrometer in the range of 400-4000 cm^{-1}. Thermal analyses were performed on a METTLER TOLEDO TGA/DSC 1 instrument in the range of 30-800 °C with Al_2O_3 pan at a heating rate of 5 ºC/min. Powder X-ray diffraction data were collected using a Bruker D8 ADVANCE PXRD equipped with a CuKα X-ray source over the 2θ range of 5 to 50° at room temperature. The magnetic susceptibility data were obtained on a Quantum Design MPMS3 SQUID system. The direct current measurements were obtained with an external magnetic field of 1.0 kOe in the temperature range 1.8-300 K, and the alternating-current measurements were executed in a 2.0 Oe *ac* oscillating field at different frequencies from 0.1 to 1000 Hz. The diamagnetic contribution of the sample itself was estimated from Pascal's constant.[S1]

S2 X-ray crystallography

Diffraction intensity data of $\mathbf{Dy_{16}K_{12}}$ and $\mathbf{Dy_{24}Na_{44}}$ were recorded on a ROD, XtaLAB Synergy, Dualflex, HyPix diffractometer using Cu Kα (λ = 1.54184 Å) at 100(1) K. Their structures were resolved and refined by using the SHELX-2018 program.[S2] For $\mathbf{Dy_{16}K_{12}}$ and $\mathbf{Dy_{24}Na_{44}}$, all non-H atoms were refined with anisotropic displacement parameters. The H atoms in the whole structure were geometrically fixed. Crystallographic data are listed in Table 1. The bond lengths, bond angles and H bonds are summarized in Table S1-S4. CCDC 2456379 ($\mathbf{Dy_{16}K_{12}}$) and CCDC 2456380 ($\mathbf{Dy_{24}Na_{44}}$) contain the supplementary crystallographic data for this paper. These data can be obtained free of charge from the Cambridge Crystallographic Data Centre via www.ccdc.cam.ac.uk/data_request/cif.

S3 Structure information

(a) **(b)**

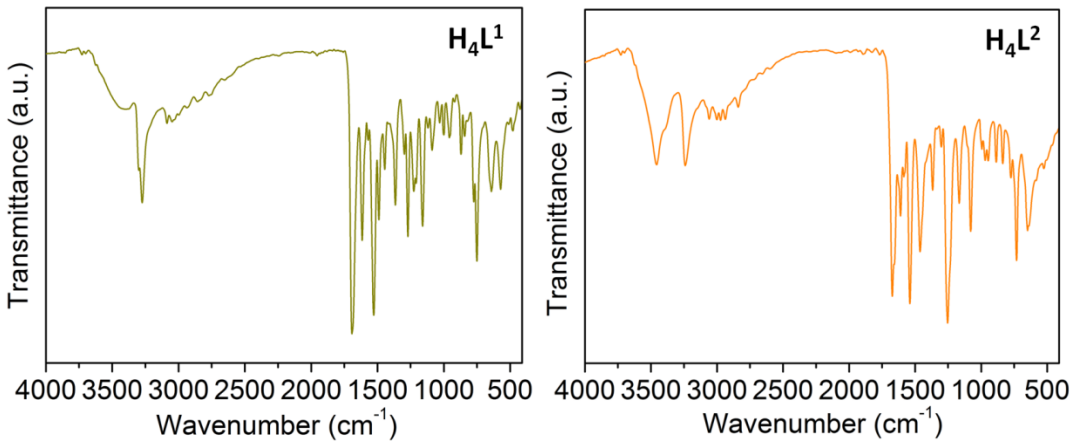

Figure S1. Infrared spectra of H_4L^1 (a) and H_4L^2 (b).

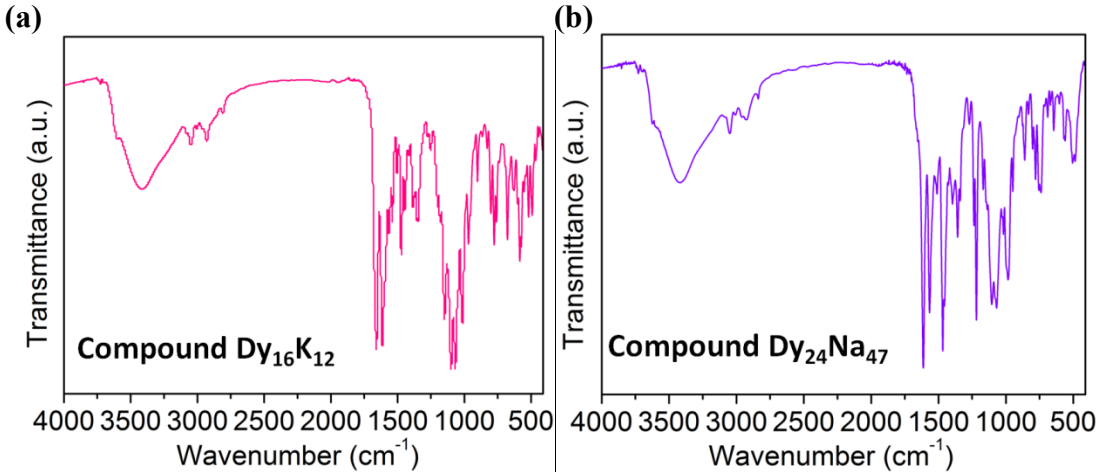

Figure S2. Infrared spectra of compounds $Dy_{16}K_{12}$ (a) and $Dy_{24}Na_{44}$.

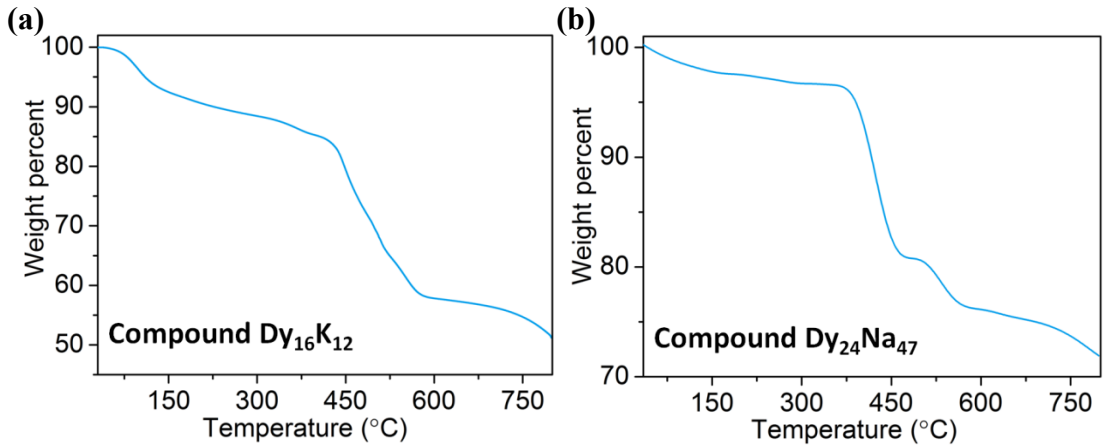

Figure S3. Thermal analysis of compounds $Dy_{16}K_{12}$ (a) and $Dy_{24}Na_{44}$ (b).

(a) **(b)**

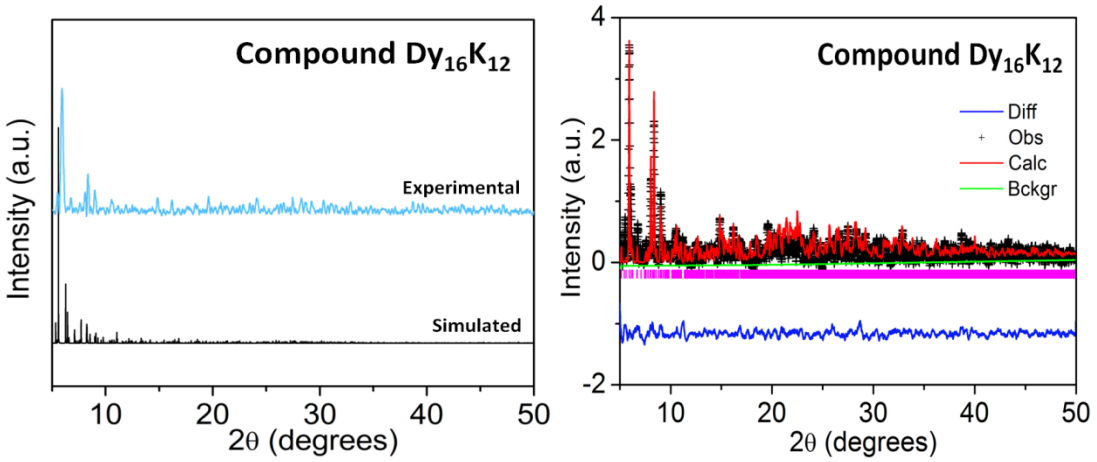

Figure S4. The powder XRD patterns of compound **$Dy_{16}K_{12}$** (a). The black circles are for the observed data (b). The red solid line is for the calculated data. The grey solid curve is for the difference. The vertical bars are the positions of Bragg peaks. Cell parameters: *R*-3*c*, a = 48.9298(8) Å, b = 48.9298(8) Å, c = 109.1024(3) Å, $\alpha = 90°$, $\beta = 90°$, $\gamma = 120°$, V = 204065.86(1) Å^3 (wRp = 0.046).

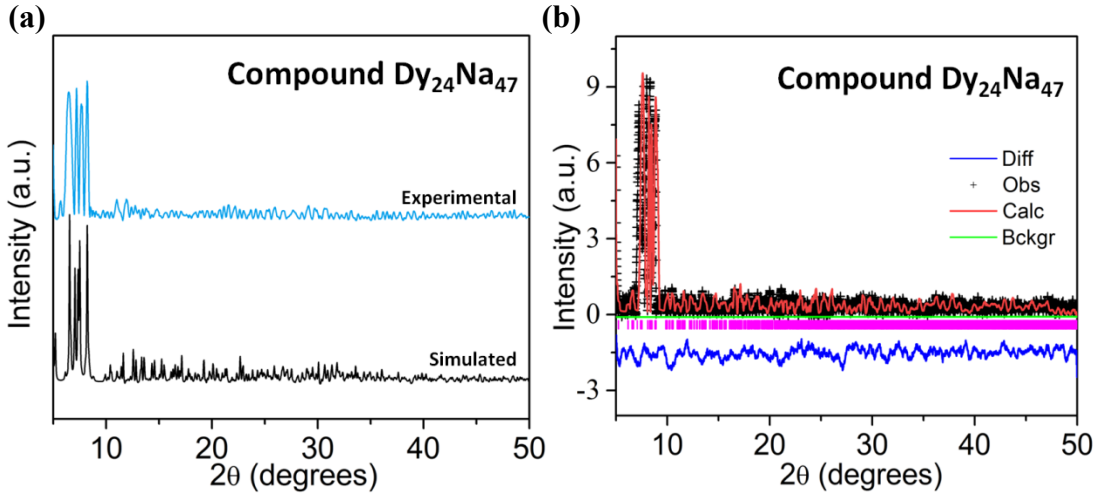

Figure S5. The powder XRD patterns of compound **$Dy_{24}Na_{44}$** (a). The black circles are for the observed data (b). The red solid line is for the calculated data. The grey solid curve is for the difference. The vertical bars are the positions of Bragg peaks. Cell parameters: *P*2/*n*, a = 33.8050(1) Å, b = 33.8050(1) Å, c = 26.9287(6) Å, $\alpha = 90°$, $\beta = 90°$, $\gamma = 90°$, V = 30961.55(9) Å^3 (wRp = 0.058).

(a) (b)

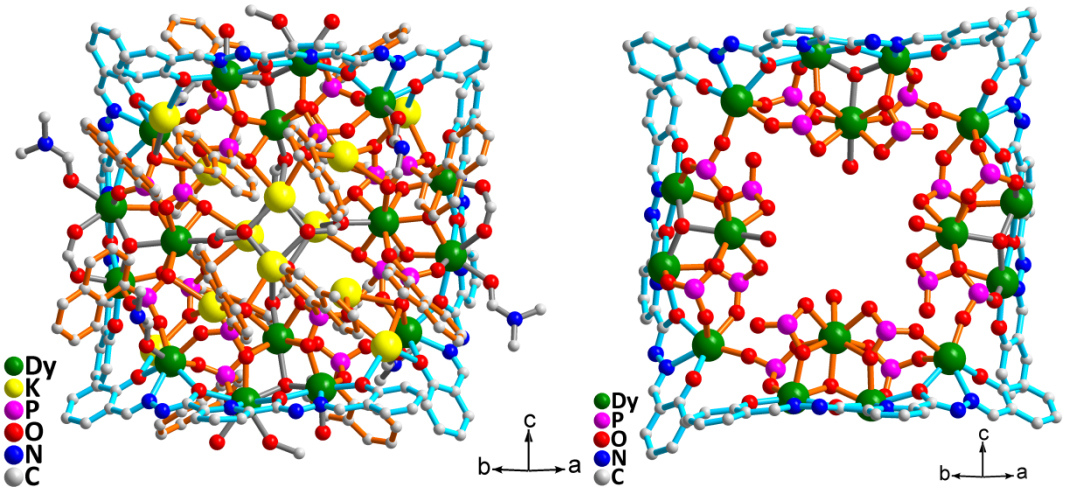

Figure S6. Ball-and-stick views of compound $\mathbf{Dy_{16}K_{12}}$ (a). Highlighting the $[Dy_{16}(L^1)_4(O_3P)_{16}(\mu_3\text{-}O)_4(\mu\text{-}O)_4]^{12-}$ fragment (b). The menaphthyl and ethyl groups, and the coordinating DMF, MeCN and H_2O molecules, and hydrogen atoms are omitted for clarity.

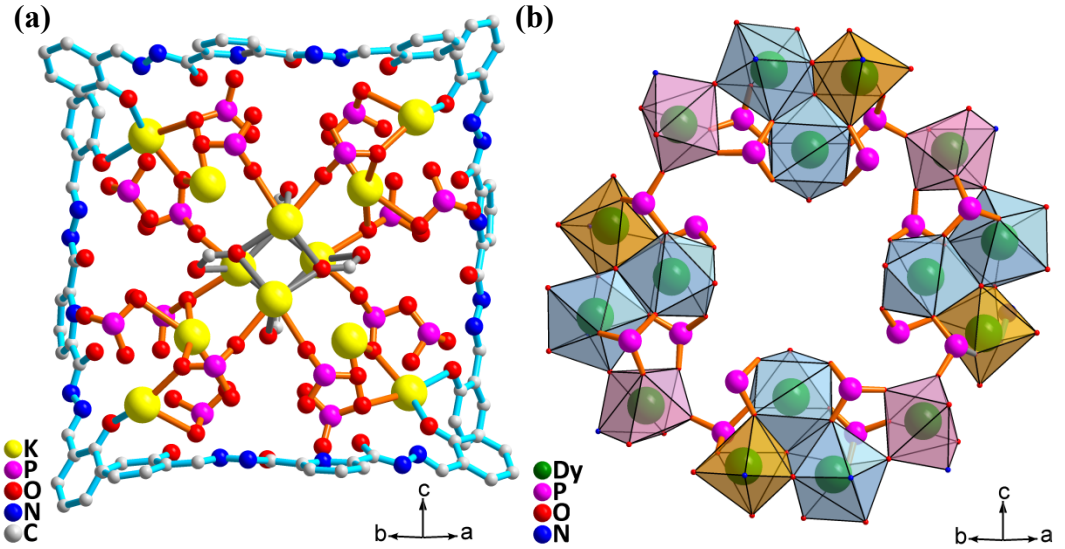

Figure S7. Highlighting the $[K_{12}(L^1)_4(O_3P)_{16}(\mu_3\text{-}COO)_4]^{40-}$ fragment (a). The menaphthyl and ethyl groups, and the coordinating DMF, MeCN and H_2O molecules, and hydrogen atoms are omitted for clarity. Coordination polyhedra observed for the metal centers of compound $\mathbf{Dy_{16}K_{12}}$ (b).

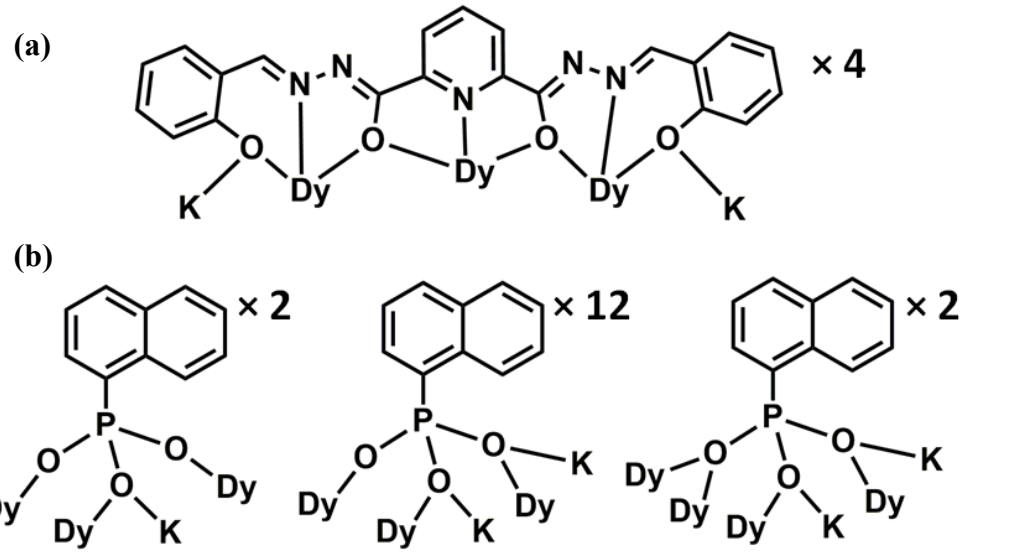

Figure S8. The coordination modes of the L^1 (a) and 1-naphthylphosphonate (b) ligands.

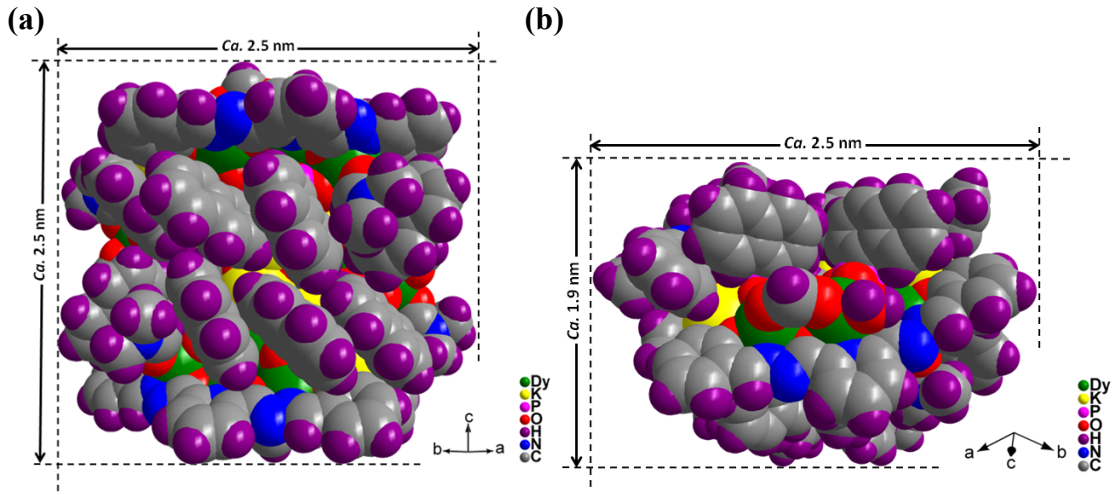

Figure S9. Space-filling representation of compound $\mathbf{Dy_{16}K_{12}}$ (a and b).

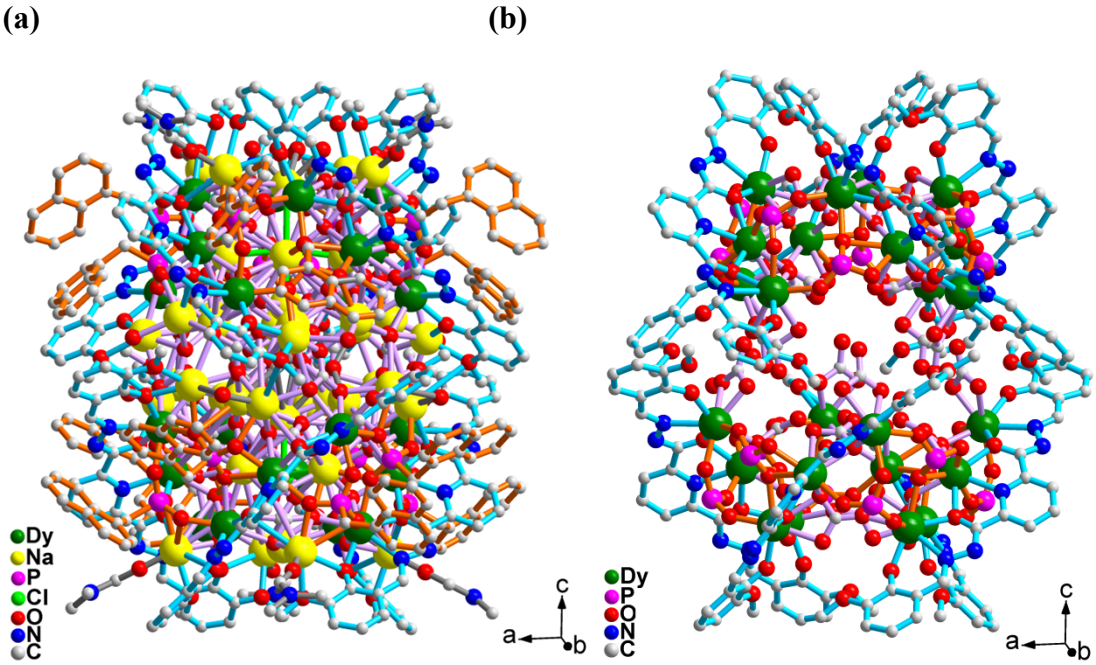

Figure S10. Ball-and-stick views of compound $\mathbf{Dy_{24}Na_{44}}$ (a). Highlighting the $[Dy_{24}(L^2)_8(O_3P)_{16}(CO_3)_{19}]^{30+}$ fragment (b). The menaphthyl and ethyl groups, and the coordinating DMF, MeCN and H_2O molecules, and hydrogen atoms are omitted for clarity..

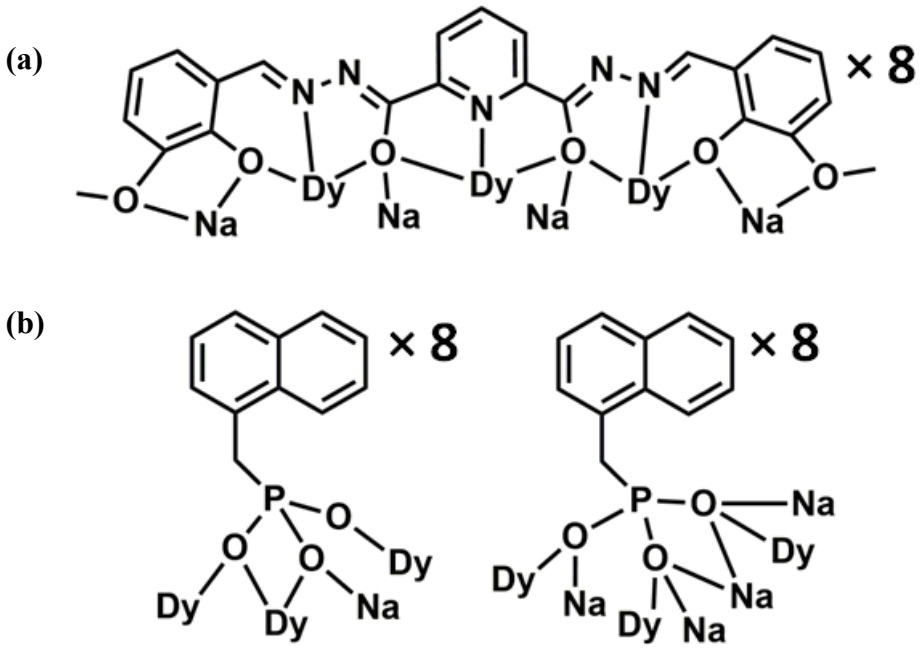

Figure S11. The coordination modes of the L^2 (a) and 1-naphthylmethylphosphonate (b) ligands.

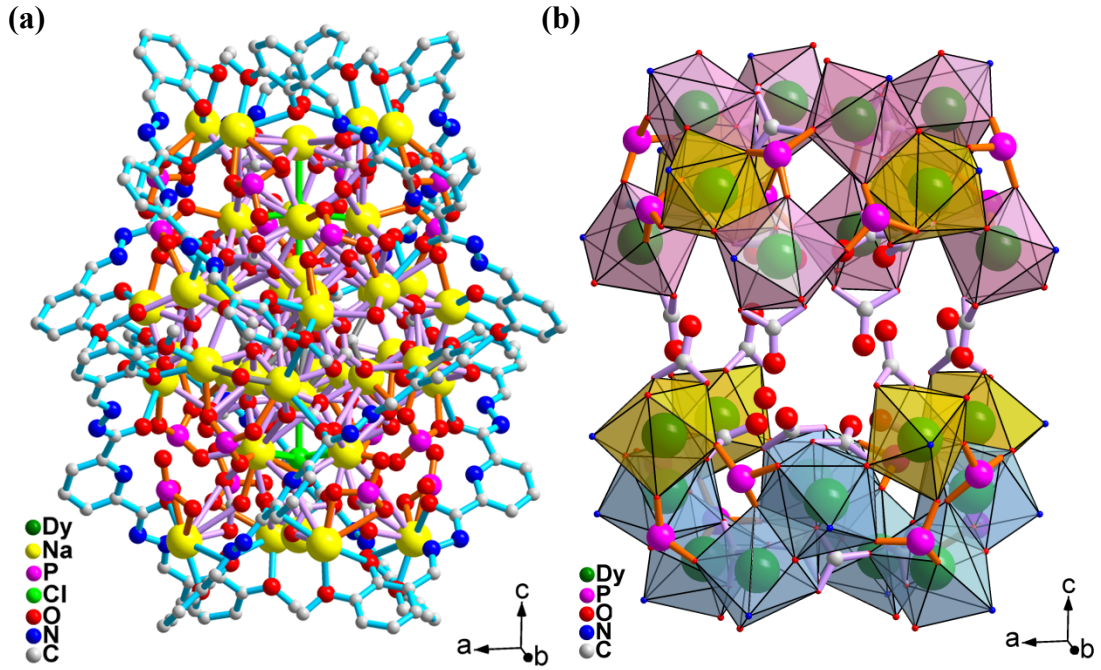

Figure S12. Highlighting the $[Na_{44}(L^2)_8(O_3P)_{16}(CO_3)_{25}(Cl)_2(\mu_2\text{-}OH)_8]^{72-}$ fragment (a). The menaphthyl and ethyl groups, and the coordinating DMF, MeOH and H_2O molecules, and hydrogen atoms are omitted for clarity. Coordination polyhedra observed for the metal centers of compound **$Dy_{24}Na_{44}$** (b).

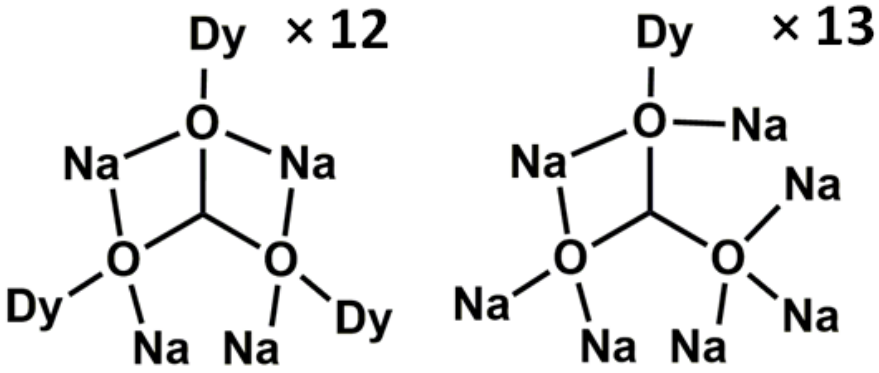

Figure S13. The coordination modes of the carbonate anions.

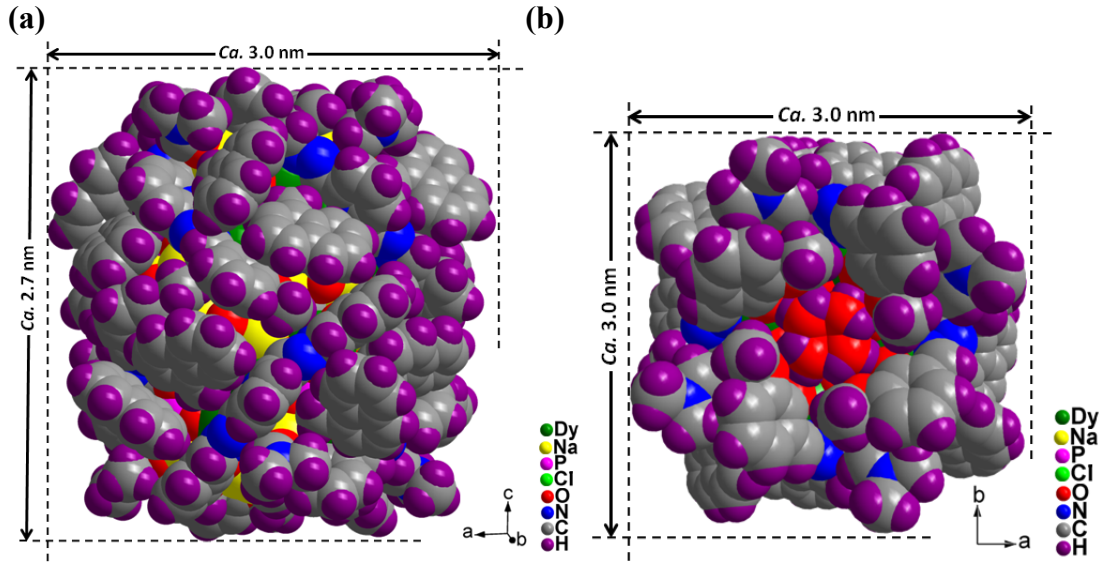

Figure S14. Space-filling representation of compound $Dy_{24}Na_{44}$ (a and b).

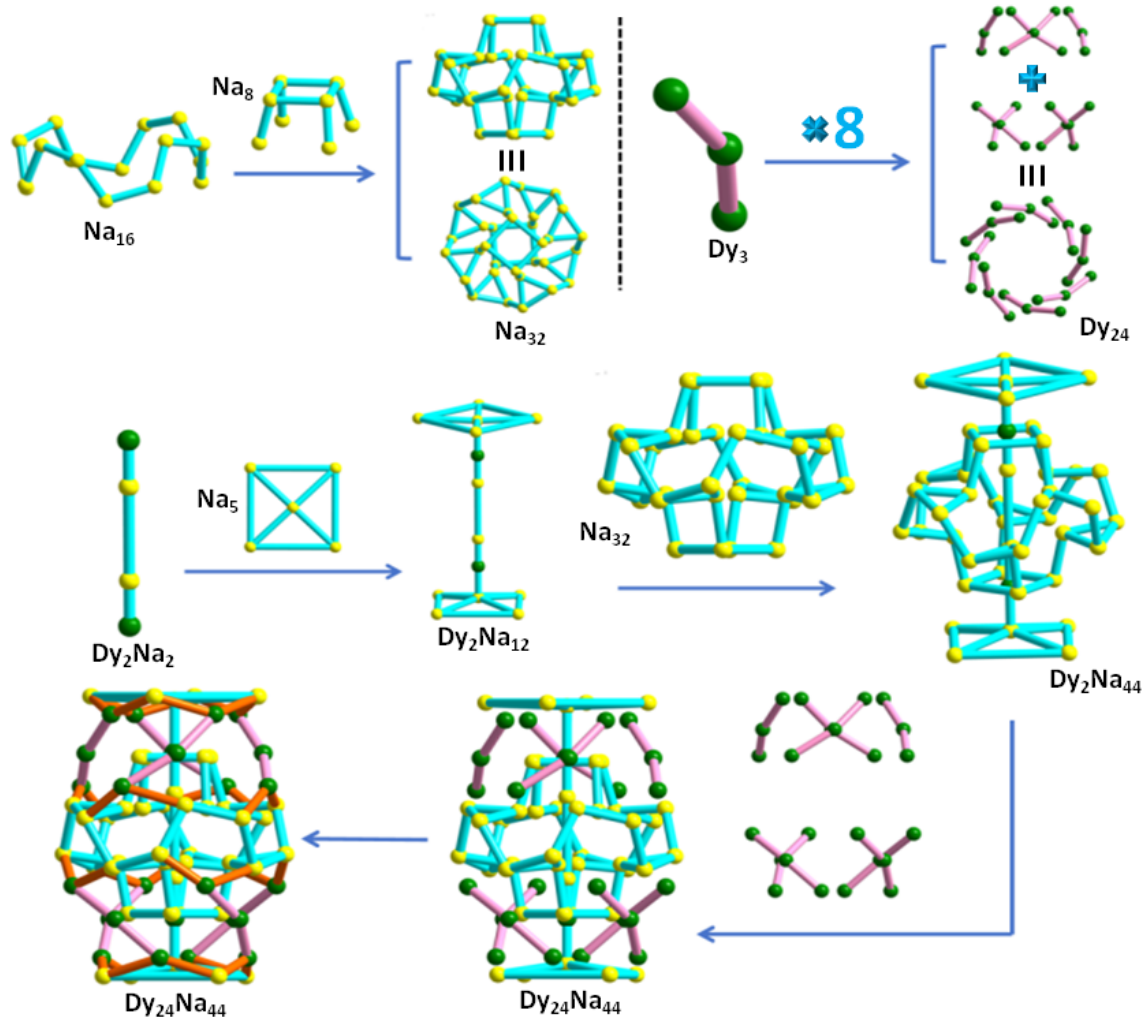

Figure S15. Dissect the inorganic core motif of compound $Dy_{24}Na_{44}$ into three concentric barrel-shaped shells.

Table S1. Selected bond lengths (Å) and angles (º) for compound $\mathbf{Dy_{16}K_{12}}$.

Compound $Dy_{16}K_{12}$					
Dy1-N1	2.587	Dy1-O1	2.248(2)	Dy1-O10	2.249
Dy1-O2	2.419(9)	Dy1-O3	2.353	Dy1-O4	2.292(1)
Dy1-O44a	2.283(3)	Dy2-N3	2.473(5)	Dy2-O2	2.389(8)
Dy2-O3	2.360(4)	Dy2-O5	2.361(2)	Dy2-O6	2.458(2)
Dy2-O7	2.455(6)	Dy2-O8	2.248(5)	Dy2-O9	2.314(7)
Dy3-N5	2.522(1)	Dy3-O11	2.276(9)	Dy3-O15	2.287(7)
Dy3-O16	2.234	Dy3-O17	2.338(1)	Dy3-O18	2.240(1)
Dy3-O7	2.383(4)	Dy4-O24	2.253(5)	Dy4-O25	2.25
Dy4-O26	2.315(3)	Dy4-O27	2.411(9)	Dy4-O29	2.341(9)
Dy4-O30	2.261(1)	Dy4-N7	2.529	Dy5-O20	2.374(5)
Dy5-O21	2.288	Dy5-O22	2.385(7)	Dy5-O27	2.355(4)
Dy5-O30	2.560(8)	Dy5-O33	2.410(6)	Dy5-O34	2.323(4)
Dy5-O35	2.433(3)	Dy6-N9	2.477	Dy6-O27	2.347(9)
Dy6-O28	2.418(9)	Dy6-O29	2.338(7)	Dy6-O35	2.336(7)
Dy6-O36	2.236(2)	Dy6-O37	2.433(6)	Dy6-O38	2.456(3)
Dy7-N12	2.507	Dy7-O38	2.401(2)	Dy7-O39	2.280(3)
Dy7-O40	2.263(6)	Dy7-O43	2.282(7)	Dy7-O45	2.250(6)
Dy7-O46	2.305	Dy8-O2a	2.394	Dy8-O41	2.378(3)
Dy8-O42	2.262(4)	Dy8-O9a	2.429(9)	Dy8-O10a	2.531(8)
Dy8-O12a	2.394(7)	Dy8-O14a	2.367(1)	Dy8-O31a	2.319(3)
Dy1-O2-Dy2	109.54	Dy1-O2-Dy8a	105.69	Dy1-O3-Dy2	112.92
Dy1-O10-Dy8a	106.59	Dy1a-O44-K6	98.33	Dy2-O9-Dy8a	107.56
Dy2-O7-Dy3	128.43	Dy2-O2-Dy8a	106.31	Dy3-O15-K1	92.59
Dy3-O15-K2	97.63	Dy3-O16-K1	96.00	Dy3-O18-K1	91.39
Dy3-O18-K2	99.18	Dy4-O24-K1	103.29	Dy4-O27-Dy5	108.78
Dy4-O27-Dy6	108.15	Dy4-O29-Dy6	110.88	Dy4-O30-Dy5	106.83
Dy4-O25-K1	99.74	Dy5-O27-Dy6	109.27	Dy5-O33-K4	95.91
Dy5-O33-K5	100.03	Dy5-O34-K5	103.66	Dy5-O35-Dy6	107.03
Dy6-O38-Dy7	132.18	Dy7-O39-K5	93.41	Dy7-O39-P6	144.85
Dy7-O40-K5	96.50	Dy7-O40-K6	92.70	Dy7-O43-K5	94.70
Dy7-O43-K6	88.82	Dy7-O45-K6	95.10	Dy8-O41-K2a	92.69
Dy8-O41-K3a	93.21	Dy8-O42-K5	106.06	Dy8a-O12-K2	96.30
Dy8a-O12-K3	91.33	Dy8a-O14-K3	99.01	Dy8a-O14-K5a	104.72

Symmetry codes: a: x, y, 1/2-z.

Table S2. Selected bond lengths (Å) and angles (º) for compound $\mathbf{Dy_{24}Na_{44}}$.

Compound $Dy_{24}Na_{44}$					
Dy1-N1a	2.535(6)	Dy1-O10a	2.586(5)	Dy1-O11	2.300(5)
Dy1-O13	2.241(5)	Dy1-O2a	2.244(6)	Dy1-O4a	2.458(5)
Dy1-O8a	2.382(5)	Dy1-O9a	2.311(5)	Dy2-N4	2.484(6)
Dy2-O10	2.327(5)	Dy2-O14	2.278(5)	Dy2-O16	2.346(5)
Dy2-O18	2.363(5)	Dy2-O5a	2.469(5)	Dy2-O6a	2.481(5)
Dy2-O8	2.608(5)	Dy2-O9	2.391(5)	Dy3-N6	2.546(5)
Dy3-O15	2.253(5)	Dy3-O17a	2.376(5)	Dy3-O18	2.470(5)
Dy3-O22	2.474(5)	Dy3-O23	2.332(5)	Dy3-O24	2.256(5)
Dy3-O6a	2.405(5)	Dy4-O19	2.468(5)	Dy4-O31	2.352(5)
Dy4-O41	2.246(5)	Dy4-N7c	2.538(6)	Dy4-O27c	2.284(5)
Dy4-O34c	2.385(4)	Dy4-O35c	2.448(5)	Dy4-O36a	2.391(4)
Dy5-N9c	2.512(5)	Dy5-O33c	2.458(5)	Dy5-O34c	2.483(4)
Dy5-O35c	2.384(5)	Dy5-O37	2.369(5)	Dy5-O38	2.628(4)
Dy5-O39	2.335(5)	Dy5-O40	2.246(5)	Dy5-O44c	2.360(5)
Dy6-N11	2.565(6)	Dy6-O38a	2.400(5)	Dy6-O39a	2.592(4)
Dy6-O42	2.318(5)	Dy6-O43	2.235(5)	Dy6-O44	2.322(5)
Dy6-O45	2.238(5)	Dy6-O47a	2.439(5)	Dy1c-O2-Na1c	96.5(2)
Dy1c-O4-Na1	112.7(2)	Dy1c-O8-Dy2	96.77(16)	Dy1c-O8-Na3	88.57(17)
Dy1c-O9-Dy2	105.1(2)	Dy1c-O10-Na3	86.56(16)	Dy1c-O10-Dy2	98.78(16)
Dy1-O11-Na3a	89.81(17)	Dy2c-O5-Na3c	89.66(16)	Dy2c-O5-Na4c	154.5(2)
Dy2c-O5-Na6c	85.37(15)	Dy2c-O6-Dy3c	106.70(17)	Dy2c-O6-Na3	115.2(2)
Dy2-O8-Na3	90.90(16)	Dy2-O10-Na3	101.57(19)	Dy2-O14-Na1	116.1(2)
Dy2-O16-Na6	93.98(17)	Dy2-O18-Dy3	108.38(17)	Dy3c-O6-Na3	124.76(19)
Dy3c-O17-Na8	93.54(18)	Dy3-O22-Na6	109.7(2)	Dy3-O22-Na7	152.3(2)
Dy3-O23-Na4a	120.0(2)	Dy3-O23-Na8a	92.47(18)	Dy3-O24-Na8a	94.75(18)
Dy4-O19-Na9c	111.5(2)	Dy4-O19-Na8	154.9(2)	Dy4a-O27-Na7a	93.69(17)
Dy4-O31-Na10	118.1(2)	Dy4-O31-Na7	90.68(16)	Dy4a-O34-Dy5a	106.86(16)
Dy4a-O34-Na12b	128.32(19)	Dy4a-O35-Dy5a	108.03(17)	Dy4c-O36-Na7c	91.83(17)
Dy5a-O33-Na10	149.2(2)	Dy5a-O33-Na9	87.05(15)	Dy5a-O34-Na12b	114.02(19)
Dy5-O37-Na9c	92.62(17)	Dy5-O38-Dy6c	95.91(15)	Dy5-O38-Na12	93.96(16)
Dy5-O39-Dy6c	98.56(15)	Dy5-O39-Na12	103.14(19)	Dy5-O40-Na15	122.6(5)
Dy5-O40-Na13	113.6(3)	Dy5a-O44-Dy6	105.93(18)	Dy6c-O47-Na13	106.1(3)
Dy6c-O47-Na15	120.0(5)	Dy6c-O38-Na12	88.35(16)	Dy6c-O39-Na12	84.75(14)
Dy6-O42-Na12a	88.54(17)	Dy6-O43-Na15	87.3(5)	Dy6-O45-Na15	90.2(4)

Symmetry codes: a: x, 1/2-y, z; b: 1/2-x, 1/2-y, z; c: 1/2-x, y, z.

Table S3. Hydrogen bonds for compound $Dy_{16}K_{12}$.

Compound $Dy_{16}K_{12}$				
D–H···A	**d(D–H) (Å)**	**d(H···A) (Å)**	**d(D···A) (Å)**	**<(DHA) (°)**
C16-H16···O14	0.9500	2.5000	2.9601	110.00
C27-H27a···O9	0.9500	2.4600	2.9328	111.00
C37-H37···O15	0.9500	2.4500	3.0228	119.00
C44-H44···O31	0.9500	2.5400	2.9863	109.00
C64-H64···O21	0.9500	2.4900	2.9298	108.00
C81-H81···O30	0.9500	2.4500	2.9095	110.00
C88-H88···O28	0.9500	2.4000	3.3448	175.00
C94-H94···O35	0.9500	2.4600	2.9142	109.00
C101-H101···O39	0.9500	2.3800	3.0172	124.00
C104-H104···O34	0.9500	2.5300	2.9570	107.00
C109-H109···O28	0.9500	2.5300	3.3308	143.00
C111-H111···O36	0.9500	2.5100	3.1674	127.00
C112-H112···O38	0.9500	2.5500	2.9801	107.00
C128-H128···O42	0.9500	2.4500	2.9029	109.00

Symmetry codes: a: x, y, 1/2-z.

Table S4. Hydrogen bonds for compound $Dy_{24}Na_{44}$.

Compound $Dy_{24}Na_{44}$				
D–H···A	**d(D–H) (Å)**	**d(H···A) (Å)**	**d(D···A) (Å)**	**<(DHA) (°)**
O3-H3a···O11	0.8700	2.3900	2.9011	117.00
O3-H3a···O2	0.8700	1.7400	2.4899	143.00
O3-H3a···O4	0.8700	2.3700	2.7731	109.00
O3-H3b···O1	0.8700	2.3300	2.9083	124.00
O3-H3b···O4	0.8700	1.9300	2.4221	115.00
O21-H21a···O27	0.8600	2.3600	3.1077	145.00
O46-H46a···O47	0.8700	1.6900	2.3618	132.00
O46-H46a···O48	0.8700	2.1600	2.6339	113.00
O46-H46b···O45	0.8700	1.6500	2.3328	140.00
O46-H46b···O47	0.8700	2.4200	2.9868	123.00
C4-H4a···O12	0.9900	2.5200	3.4611	158.00
C37-H37c···N7	0.9800	2.5900	3.2862	129.00
C45-H45···O16	0.9500	2.4900	3.0248	116.00
C79-H79b···O49	0.9900	2.5800	3.4639	148.00
C86-H86···N8	0.9500	2.5700	3.3792	144.00
C90-H90a···O43	0.9900	2.5700	3.3619	137.00

Symmetry codes: a: x, y, 1/2-z; b: 2/3-x, 1/3+y, 2/3-z; c: -1/3+x, 1/3 -y, 2/3-z.

Table S5. Dy^{III} geometry analysis of $\mathbf{Dy_{16}K_{12}}$ by SHAPE 2.1 software.

Compound $Dy_{16}K_{12}$									
Geometry (CN = 7)	**Dy1**	**Dy5**	**Dy6**	**Dy7**	**Geometry (CN = 8)**	**Dy2**	**Dy3**	**Dy4**	**Dy8**
HP-7	32.324	32.84	32.017	32.066	**OP-8**	29.988	30.53	30.543	31.567
HPY-7	18.833	20.3374	19.664	20.392	**HPY-8**	23.972	24.03	24.631	24.491
PBPY-7	5.631	1.973	1.46	4.315	**HBPY-8**	16.091	16.265	16.575	16.031
COC-7	0.986	4.737	5.71	1.437	**CU-8**	12.904	13.166	12.167	11.77
CTPR-7	1.553	3.979	4.534	1.885	**SAPR-8**	2.812	3.348	2.826	3.531
JPBPY-7	8.842	4.705	4.033	7.792	**TDD-8**	2.044	2.384	1.697	1.117
JETPY-7	17.503	19.065	20.729	18.009	**JGBF-8**	13.014	12.483	13.398	11.58
					JETBPY-8	27.108	27.591	27.895	27.056
					JBTPR-8	1.921	2.989	2.797	2.735
					BTPR-8	1.206	2.240	2.370	2.304
					JSD-8	3.501	4.521	3.987	2.986
					TT-8	13.651	13.735	12.909	12.508
					ETBPY-8	23.640	23.256	23.090	23.900

Table S6. Dy^{III} geometry analysis of $\mathbf{Dy_{24}Na_{44}}$ by SHAPE 2.1 software.

Compound $Dy_{24}Na_{44}$							
Geometry (CN = 8)	**Dy1**	**Dy3**	**Dy4**	**Dy6**	**Geometry (CN = 9)**	**Dy2**	**Dy5**
OP-8	32.173	31.431	31.897	32.574	**EP-9**	33.348	34.008
HPY-8	22.981	23.355	23.04	23.539	**OPY-9**	21.419	21.082
HBPY-8	14.245	13.338	13.424	14.334	**HBPY-9**	15.606	15.435
CU-8	9.783	9.792	9.986	9.639	**JTC-9**	13.373	13.765
SAPR-8	5.276	2.917	3.094	4.765	**JCCU-9**	8.778	9.339
TDD-8	2.836	2.764	2.596	2.445	**CCU-9**	8.086	8.587
JGBF-8	12.291	11.329	11.309	13.265	**JCSAPR-9**	2.698	2.592
JETBPY-8	25.416	26.757	26.161	25.475	**CSAPR-9**	1.769	1.605
JBTPR-8	3.696	2.737	2.872	3.360	**JTCTPR-9**	2.706	3.160
BTPR-8	3.000	1.652	1.834	2.688	**TCTPR-9**	2.539	2.745
JSD-8	6.017	3.697	3.532	5.492	**JTDIC-9**	12.463	12.678

TT-8	10.357	10.186	10.347	10.231	**HH-9**	8.815	9.111
ETBPY-8	20.447	22.074	22.095	20.553	**MFF-9**	1.608	1.437

S4 Magnetic properties

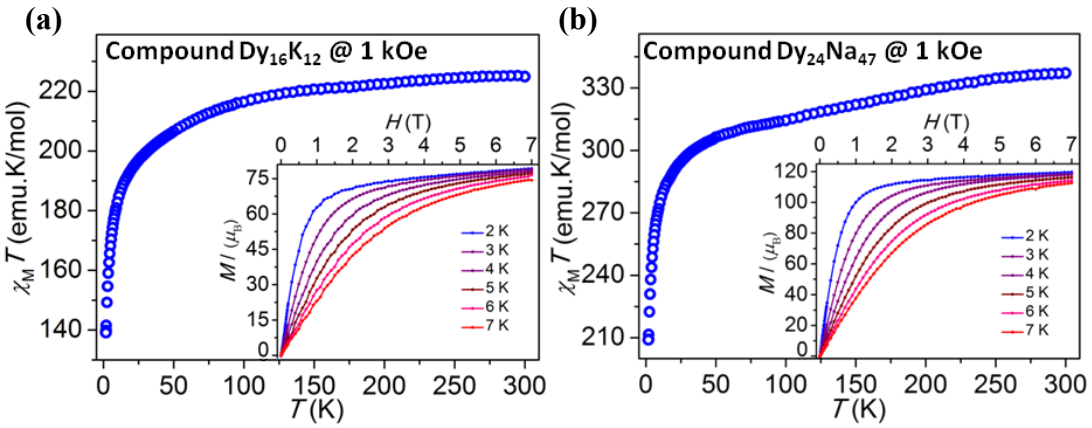

Figure S16. Temperature dependent of the $\chi_M T$ values at 1.0 kOe for compounds **$Dy_{16}K_{12}$** (a) and **$Dy_{24}Na_{44}$** (b). Inset: the magnetization *vs.* field plots at different temperature.

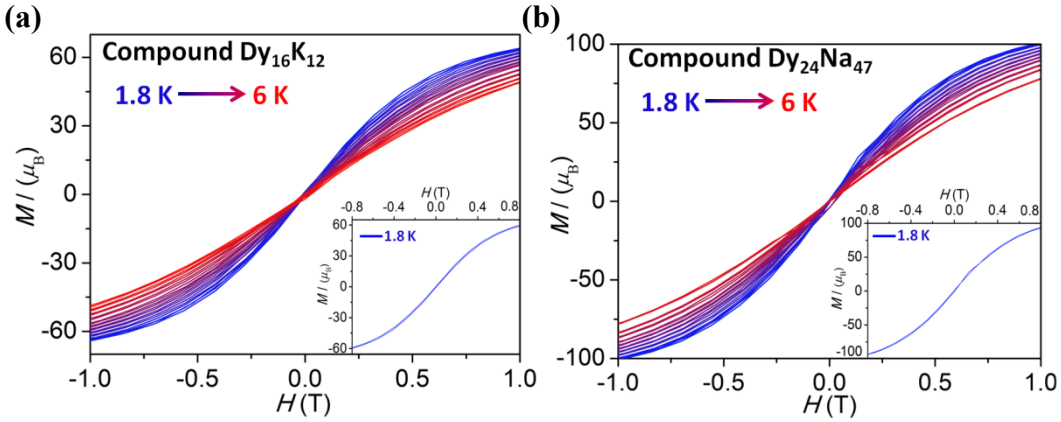

Figure S17. Variable-field magnetization data collected for compounds **$Dy_{16}K_{12}$** (a) and **$Dy_{24}Na_{44}$** (b) at an average field sweep rate of 100 Oe/s. Inset shows a view of the plot at 1.8 K.

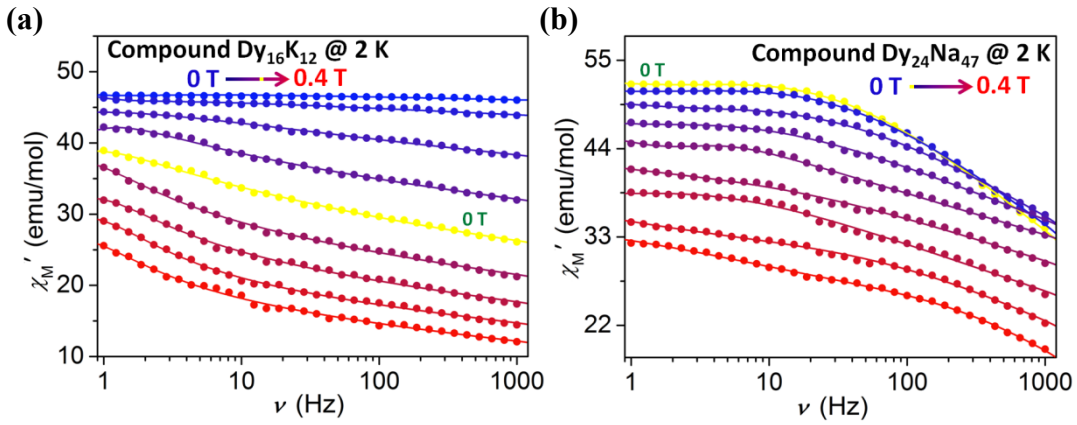

Figure S18. Variable-field χ_M' magnetic susceptibility versus frequency data for compounds **$Dy_{16}K_{12}$** (a) and **$Dy_{24}Na_{44}$** (b), collected at fields ranging from 0 to 0.4 T at 2.0 K.

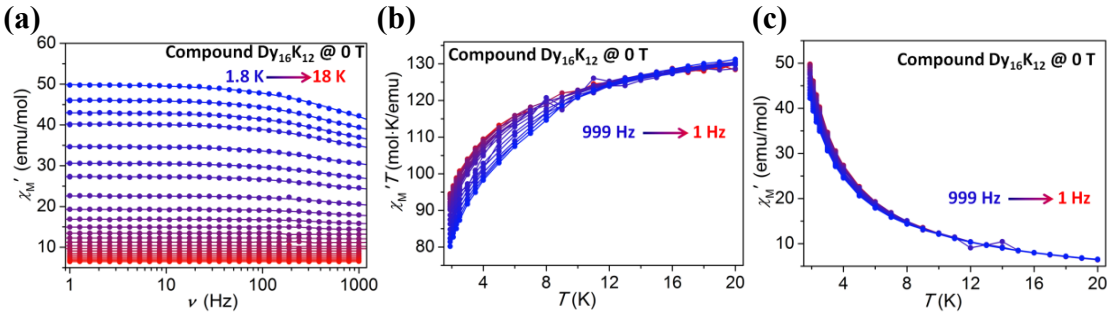

Figure S19. Variable-temperature χ_M' magnetic susceptibility versus frequency data for compound **$Dy_{16}K_{12}$** under zero applied dc field, collected at temperatures ranging from 1.8 to 18 K (a). Variable-frequency $\chi_M'T$ (b) and χ_M' (c) magnetic susceptibility versus temperature data under zero applied dc field, collected at frequencies from 1 to 999 Hz.

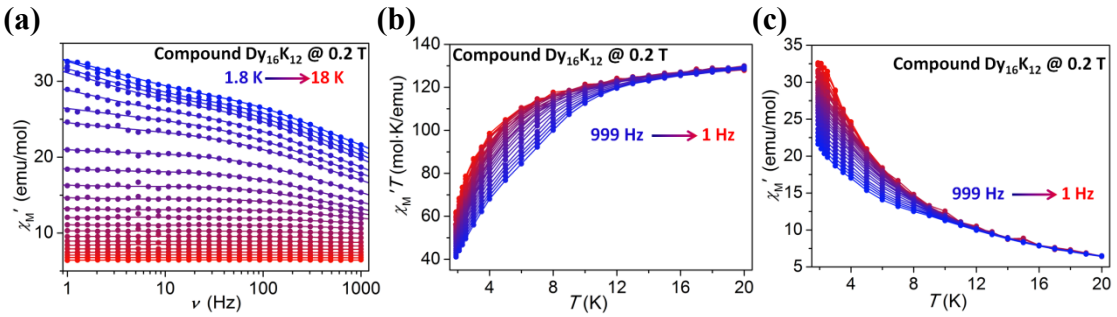

Figure S20. Variable-temperature χ_M' magnetic susceptibility versus frequency data for compound **$Dy_{16}K_{12}$** under the optimal 0.2 T dc field, collected at temperatures ranging from 1.8 to 18 K (a). Variable-frequency $\chi_M'T$ (b) and χ_M' (c) magnetic susceptibility versus temperature data under the optimal 0.2 T dc field, collected at frequencies from 1 to 999 Hz.

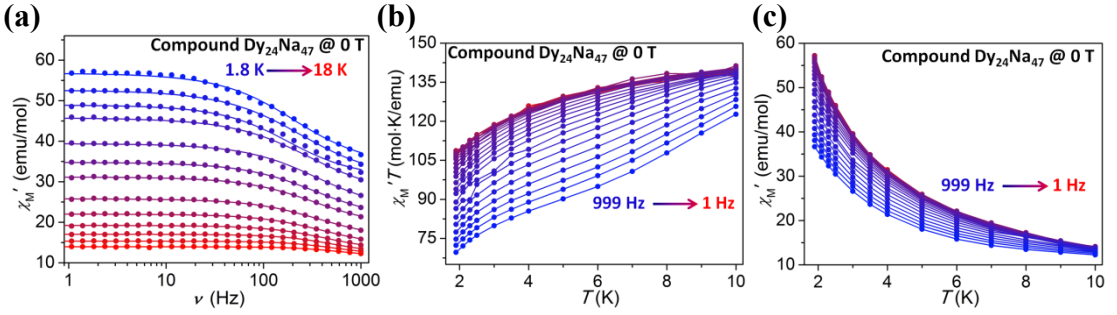

Figure S21. Variable-temperature χ_M' magnetic susceptibility versus frequency data for compound **$Dy_{24}Na_{44}$** under zero applied dc field, collected at temperatures ranging from 1.8 to 18 K (a). Variable-frequency $\chi_M'T$ (b) and χ_M' (c) magnetic susceptibility versus temperature data under zero applied dc field, collected at frequencies from 1 to 999 Hz.

Table S7. Parameters used to fit temperature-dependent relaxation times for **$Dy_{16}K_{12}$** under zero applied dc field.

Faster relaxation				
Magnetic relaxation pathway	**τ_{tunnel} (s)**	**C ($s^{-1}K^{-n}$)**	**n**	**A ($s^{-1}K^{-n}$)**
Direct process	--	--	--	$6.87(2) \times 10^{-3}$
Raman process	--	$7.90(1) \times 10^{-2}$	4.59(5)	--
QTM process	$3.68(6) \times 10^{-4}$	--	--	--
Direct, Raman and QTM processes	$6.32(2) \times 10^{-4}$	$8.60(5) \times 10^{-2}$	7.22(4)	$5.49(6) \times 10^{-3}$

Table S8. Parameters used to fit temperature-dependent relaxation times for **$Dy_{16}K_{12}$** under the optimal 0.2 T dc field.

Slower relaxation						
Magnetic relaxation pathway	**τ_{tunnel} (s)**	**C ($s^{-1}K^{-n}$)**	**n**	**A ($s^{-1}K^{-n}$)**	**τ_0 (s)**	**U_{eff} (K)**
Orbach process	--	--	--	--	$5.29(1) \times 10^{-7}$	38.62(5)
Raman process	--	$2.27(8) \times 10^{-2}$	6.26(1)	--	--	--
Direct process	--	--	--	$4.15(2) \times 10^{-3}$	--	--
QTM process	$3.37(5) \times 10^{-4}$	--	--	--	--	--
Orbach, Raman, Direct and QTM processes	$7.86(4) \times 10^{-4}$	$4.58(4) \times 10^{-2}$	6.91(4)	$9.82(1) \times 10^{-3}$	$1.65(4) \times 10^{-7}$	23.39(6)
Faster relaxation						
Magnetic relaxation pathway	**τ_{tunnel} (s)**					
QTM process	$1.03(5) \times 10^{-4}$					

Table S9. Parameters used to fit temperature-dependent relaxation times for **$Dy_{24}Na_{44}$** under zero applied dc field.

Slower relaxation						
Magnetic relaxation pathway	**τ_{tunnel} (s)**	**C ($s^{-1}K^{-n}$)**	**n**	**A ($s^{-1}K^{-n}$)**	**τ_0 (s)**	**U_{eff} (K)**
Raman process	--	$6.71(3) \times 10^{-2}$	7.66(2)	--	--	--
Direct process	c	--	--	$4.56(6) \times 10^{-3}$	--	--
QTM process	$5.92(8) \times 10^{-4}$	--	--	--	--	--

Orbach, Raman, Direct and QTM processes	$8.91(2) \times 10^{-4}$	$4.05(8) \times 10^{-2}$	6.24(6)	$8.49(5) \times 10^{-3}$	--	--

Table S10. Magnetization relaxation fitting parameters from least-squares fitting of $\chi(\omega)$ data for compound $\mathbf{Dy_{16}K_{12}}$ under the different applied dc field.

	SR				FR		
***H* (Oe)**	$\chi_{s,\,tot}$	$\Delta\chi_1$	α_1	τ_1 / s	$\Delta\chi_2$	α_2	τ_2 / s
500	1.059(3)	9.398(2)	0.382(5)	9.473(5)E-4	59.162(1)	0.534(8)	0.010(5)
1000	2.443(3)	7.470(3)	0.320(2)	5.226(1)E-3	54.402(1)	0.487(7)	0.014(1)
1500	2.858(7)	7.238(7)	0.215(1)	9.475(9)E-3	50.260(5)	0.389(1)	0.019(9)
2000	3.656(1)	3.127(6)	0.209(9)	1.625(4)E-2	45.781(2)	0.294(4)	0.027(5)
2500	4.156(9)	2.906(8)	0.208(1)	8.421(2)E-3	40.722(4)	0.282(7)	0.032(3)
3000	5.459(4)	2.485(3)	0.180(7)	9.062(9)E-4	35.403(9)	0.271(1)	0.045(4)
3500	5.886(4)	2.396(7)	0.121(7)	1.184(6)E-4	26.095(2)	0.257(8)	0.056(3)
4000	6.307(1)	1.524(2)	0.105(8)	1.018(9)E-5	10.572(2)	0.227(6)	0.078(1)

Table S11. Magnetization relaxation fitting parameters from least-squares fitting of $\chi(\omega)$ data for compound $\mathbf{Dy_{24}Na_{44}}$ under the different applied dc field.

***H* (Oe)**	χ_T	χ_s	α	τ / s
500	97.431(5)	-23.018(7)	0.367(7)	6.832(9)E-4
1000	94.229(4)	-20.939(8)	0.350(5)	5.063(8)E-4
1500	90.834(9)	-18.302(7)	0.317(9)	2.965(1)E-4
2000	85.546(6)	-16.765(9)	0.280(1)	9.813(5)E-5
2500	81.528(1)	-14.585(1)	0.251(7)	4.695(7)E-5
3000	76.970(8)	-11.073(9)	0.235(7)	9.949(5)E-6
3500	67.570(7)	-9.793(3)	0.221(4)	6.778(6)E-6
4000	59.627(3)	-6.111(5)	0.205(3)	2.569(6)E-6

Table S12. Relaxation fitting parameters from least-squares fitting of $\chi(\omega)$ data for compound $\mathbf{Dy_{16}K_{12}}$ under zero applied dc field.

T (K)	χ_T	χ_s	α	τ / s
1.8	25.570(7)	-10.570(7)	0.361(4)	1.821(1)E-4
2.0	23.806(2)	-8.806(2)	0.360(5)	1.654(9)E-4
2.2	21.927(7)	-6.927(7)	0.359(1)	1.499(2)E-4
2.4	20.583(4)	-5.583(5)	0.355(6)	1.369(9)E-4
2.6	17.143(4)	-2.143(4)	0.342(6)	1.245(6)E-4
2.8	15.187(9)	-0.188(1)	0.336(2)	1.170(4)E-4
3.0	13.704(1)	1.295(9)	0.320(7)	1.060(4)E-4
4.0	11.922(3)	3.077(7)	0.297(4)	9.506(5)E-5
5.0	10.707(2)	4.292(8)	0.294(7)	8.566(3)E-5
6.0	10.025(8)	4.974(3)	0.286(1)	7.691(1)E-5
7.0	9.772(4)	5.227(6)	0.271(9)	6.708(2)E-5
8.0	9.571(4)	5.428(6)	0.260(9)	6.088(1)E-5
9.0	8.847(2)	6.152(8)	0.252(4)	5.191(9)E-5
10.0	8.530(8)	6.469(2)	0.249(2)	4.485(5)E-5
11.0	8.037(1)	6.962(9)	0.235(4)	4.064(7)E-5
12.0	7.820(1)	7.080(1)	0.231(2)	3.876(5)E-5
13.0	7.823(1)	7.177(1)	0.219(5)	3.668(1)E-5
14.0	7.633(2)	7.366(8)	0.193(9)	3.394(4)E-5
15.0	7.624(1)	7.976(1)	0.162(1)	3.273(8)E-5
16.0	7.423(1)	8.576(8)	0.150(5)	3.157(9)E-5
17.0	7.231(5)	8.968(5)	0.146(9)	3.075(8)E-5
18.0	7.125(9)	9.476(1)	0.141(6)	2.981(5)E-5

Table S13. The parameters obtained by fitting the Cole-Cole data of compound $\mathbf{Dy_{16}K_{12}}$ under the optimal 0.2 T dc field.

		SR			FR		
T (K)	$\chi_{s,\,tot}$	$\Delta\chi_1$	α_1	τ_1 / s	$\Delta\chi_2$	α_2	τ_2 / s
1.8	0.318(8)	15.165(1)	0.445(3)	3.636(2)E-4	64.884(7)	0.518(2)	0.136(4)
2.0	1.188(4)	13.685(2)	0.441(8)	3.554(4)E-4	56.351(4)	0.516(7)	0.137(1)
2.2	1.506(3)	13.624(4)	0.410(8)	3.487(3)E-4	52.741(3)	0.515(2)	0.139(7)
2.4	1.544(1)	13.564(9)	0.401(5)	3.391(3)E-4	49.858(4)	0.513(1)	0.137(7)
2.6	1.719(1)	13.510(7)	0.382(2)	3.382(5)E-4	46.460(5)	0.511(8)	0.137(7)
2.8	2.344(6)	13.492(1)	0.355(8)	3.302(1)E-4	44.871(5)	0.509(6)	0.136(7)
3.0	2.562(7)	12.867(1)	0.353(4)	3.279(7)E-4	41.311(8)	0.508(3)	0.135(5)
4.0	2.891(8)	12.779(5)	0.348(1)	3.135(1)E-4	39.973(8)	0.505(3)	0.136(8)
5.0	2.924(1)	12.765(8)	0.341(5)	2.761(1)E-4	36.953(7)	0.504(6)	0.136(5)
6.0	3.099(1)	12.636(9)	0.326(5)	2.166(4)E-4	32.057(9)	0.499(7)	0.136(7)
7.0	3.376(6)	12.384(7)	0.313(7)	1.824(5)E-4	30.779(4)	0.491(6)	0.135(6)
8.0	3.606(1)	12.005(2)	0.302(1)	1.418(6)E-4	28.230(6)	0.486(2)	0.137(9)
9.0	3.884(9)	11.908(3)	0.289(1)	8.560(9)E-5	25.898(2)	0.481(1)	0.137(7)
10.0	4.108(4)	11.869(2)	0.287(1)	5.447(6)E-5	21.794(6)	0.478(6)	0.135(4)
11.0	4.344(2)	11.671(2)	0.286(6)	3.804(9)E-5	19.859(2)	0.475(8)	0.136(4)
12.0	4.577(8)	11.658(1)	0.285(1)	2.864(5)E-5	16.172(3)	0.466(4)	0.137(9)
13.0	4.770(6)	11.632(5)	0.284(9)	2.240(4)E-5	14.146(1)	0.454(9)	0.135(9)
14.0	4.967(4)	11.552(1)	0.283(8)	1.746(1)E-5	12.785(3)	0.444(2)	0.135(8)
15.0	5.102(1)	11.254(8)	0.282(1)	1.415(6)E-5	11.779(5)	0.420(2)	0.136(8)
16.0	5.273(2)	11.082(1)	0.280(9)	1.158(4)E-5	10.642(9)	0.403(6)	0.136(8)

Table S14. Relaxation fitting parameters from least-squares fitting of $\chi(\omega)$ data for compound $\mathbf{Dy_{24}Na_{44}}$ under zero applied dc field.

T (K)	χ_T	χ_s	α	τ / s
1.8	56.819(1)	33.685(6)	0.263(9)	1.945(1)E-3
2.0	52.654(3)	30.853(1)	0.253(2)	1.829(9)E-3
2.2	48.959(7)	30.469(1)	0.238(3)	1.670(2)E-3
2.4	45.778(6)	26.600(3)	0.224(8)	1.480(7)E-3
2.6	39.430(9)	22.813(2)	0.224(7)	1.230(1)E-3
2.8	34.805(4)	20.643(3)	0.220(1)	1.080(5)E-3
3.0	31.195(5)	18.740(1)	0.205(7)	9.268(2)E-4
3.4	25.809(3)	15.827(2)	0.203(5)	7.399(5)E-4
3.8	22.034(5)	14.039(9)	0.181(9)	5.837(9)E-4
4.2	19.235(4)	12.949(9)	0.155(2)	4.550(5)E-4
4.6	17.059(3)	12.225(4)	0.112(9)	3.600(6)E-4
5.0	15.350(9)	11.959(6)	0.082(5)	3.064(2)E-4
6.0	13.963(1)	11.593(9)	0.059(3)	2.101(8)E-4

S5 REFERENCES

S1 Boudreaux, L. N. M. E. A., Theory and Applications of Molecular Paramagnetism, John Wiley & Sons, New York, **1976**.

S2 Sheldrick, G. M. Crystal structure refinement with SHELXL. *Acta Crystallogr., Sect. A: Found. Adv.* **2015**, *71*, 3−8.